

Bubble dynamics in viscoelastic fluids with application to reacting and non-reacting polymer foams

S.L. Everitt, O.G. Harlen*, H.J. Wilson, D.J. Read

Department of Applied Mathematics, University of Leeds, Leeds LS2 9JT, UK

Received 29 April 2002; received in revised form 21 March 2003

Abstract

The effects of fluid viscoelasticity on the expansion of gas bubbles in polymer foams for the cases of reactive and non-reactive polymers are investigated. For non-reactive polymers, bubble expansion is controlled by a combination of gas diffusion and fluid rheology. In the diffusion limited case, the initial growth rate is slow due to small surface area, whereas at high diffusivity initial growth is rapid and resisted only by background solvent viscosity. In this high Deborah number (De) limit, we see a two stage expansion in which there is an initial rapid expansion up to the size at which the elastic stresses balance the pressure difference. Beyond this time, the bubble expansion is controlled by the relaxation of the polymer.

In the model for reactive polymer systems, the polymer molecules begin as a mono-disperse distribution of a single reacting species. As the reaction progresses molecules bond to form increasingly large, branched, structures each with a spectrum of relaxation modes, which gel to form a viscoelastic solid. Throughout this process gas is produced as a by-product of the reaction. The linear spectrum for this fluid model is calculated from Rubinstein et al. [Dynamic scaling for polymer gelation, in: F. Tanaka, M. Doi, T. Ohta (Eds.), *Space–Time Organisation in Macromolecular Fluids*, Springer, Berlin, 1989, pp. 66–74], where the relaxation spectrum of a molecule is obtained from percolation theory and Rouse dynamics. We discretise this linear spectrum and, by treating each mode as a mode in a multimode Oldroyd-B fluid obtain a model for the non-linear rheology. Using this model, we describe how the production of gas, diffusion of gas through the liquid, and evolution of the largest molecule are coupled to bubble expansion and stress evolution. Thus, we illustrate how the rate of gas production, coupled to the rate of gas diffusion, affects the bubble size within a foam.

© 2003 Elsevier B.V. All rights reserved.

Keywords: Bubble growth; Polymer foams; Gelation; Gas diffusion; Viscoelastic; Reactive fluid

1. Introduction

Polymeric foams are used in a wide variety of applications due to their low weight, and sound- and shock-absorbing properties. There are two distinct methods of production depending on whether the

* Corresponding author. Tel.: +44-113-343-5189; fax: +44-113-343-5090.
E-mail address: oliver@maths.leeds.ac.uk (O.G. Harlen).

polymer is synthesised prior to or during the moulding process. In the former case, a polymeric liquid containing a foaming agent is injected at high pressure into a mould. As the pressure is reduced, bubbles nucleate and expand forming a polymeric foam. In the latter case of reaction injection moulding [8], liquid reactants are injected into the mould where they react forming a polymer of increasing molecular weight. Gas is produced as a by-product of the reaction, leading to the nucleation and growth of bubbles within a fluid whose rheology evolves from a low viscosity liquid to a viscoelastic gel.

There have been a number of studies of bubble growth in Newtonian fluids where bubble expansion is driven by gas diffusion. Amon and Denson [1] introduce the idea of a ‘cell model’—a spherical bubble surrounded by a spherical envelope of fluid which contains a limited supply of gas. The volume of fluid is dictated by the number of bubbles per unit volume in the cured foam. Arafmanesh and Advani [3] describe a model for bubble growth in a Newtonian fluid driven by gas diffusion. Their model takes account of heat transfer and inertia and couples bubble growth to the changing foam density. Shafi and Flumerfelt [15] describe nucleation and determination of an initial bubble radius using free energy arguments. Shafi et al. [16] follow this paper with one describing a foam made up of many spherical bubbles in ‘influence volumes’ through which gas diffuses from a limitless supply of gas dissolved in the liquid. The radius of each influence volume is dictated by the condition that the gas concentration at the outer edge is that required for nucleation.

Street [18] was one of the first to study the effects of viscoelasticity on bubble growth rate, using the Oldroyd-B fluid model. Tanasawa and Yang [19] and Ting [20] also studied bubble growth in an Oldroyd-B fluid and, like Street, assumed that all available gas was inside the bubble at nucleation. Han and Yoo [7] provide experimental results showing the effects of parameters such as injection pressure, melt elasticity, melt viscosity, diffusivity, and surface tension on bubble growth. Ramesh et al. [12] give a comparison of experimental results, their own model for bubble growth in a power law fluid and a model outlined by Arafmanesh and Advani [2] in which gas diffuses into the bubble from a limited supply dissolved in an Oldroyd-B fluid. They concluded that the Oldroyd-B model is better able to fit the experimental data, particularly in the early stages of foaming.

In order to study bubble growth in reacting polymer foams, it is necessary to model the rheology of a polymerising material as it transforms from a liquid to an elastic solid. The rheology of gelling systems near their gel point has been studied extensively by Mours and Winter [4,10,21]. Winter et al. [21] provides a detailed review of the subject, including scaling laws for the longest relaxation time, viscosity and elastic modulus of the gel. They also describe a power law molecular weight distribution and scaling of the largest molecular weight near the gel point from which they obtain the linear viscoelastic spectrum. Mours and Winter [10] compare the predictions of these scaling models with oscillatory shear experiments. Gimel et al. [6] review experiments reported in the literature to compare percolation parameters with measured data as well as performing their own simulations for the molecular weight distribution.

Rubinstein et al. [14] use a combination of percolation theory and Rouse dynamics to predict the relaxation spectrum of polydisperse self-similar molecules. They assume a power-law distribution of molecular weights between smallest and current largest molecular weights with a step function cut off at either end. The smallest molecule has a single relaxation time, with higher modes being absorbed into a solvent viscosity, while the remaining molecules each have a spectrum of relaxation modes. Randrianantoandro et al. [13] augmented Rubinstein et al.’s model by using Monte Carlo simulations to predict the form of the cut-off function at the maximum molecular weight. They also included high frequency α -relaxation in the linear relaxation spectrum. Comparisons of G' and G'' with experiment appear very good below

the gel point. Above the gel point, there is evidence of slow dynamics not captured by their model that they suggest may be due to dangling arms in the gel.

In this paper, we present two models for bubble growth in polymeric liquids. In the first model, bubble growth is driven by the diffusion of gas from a limited supply dissolved in the surrounding liquid. The fluid in this case is modelled by an Oldroyd-B fluid. Our model is similar to that of Arafmanesh and Advani [2] though we include a solvent contribution to the zero shear-rate viscosity. In the second of our two models, we take the model for polymer gelation described by Rubinstein et al. [14] and treat each of the discretised relaxation modes as a mode in a multimode Oldroyd-B fluid. We assume that gas production is proportional to the extent of reaction and that evolution of the extent of reaction follows second order kinetics. In this way, we model bubble growth, driven by gas diffusion, in a fluid with evolving rheology.

2. Non-reacting foam growth

We first consider the case of non-reacting bubble growth where foaming results from a sudden reduction in pressure that causes the blowing agent to come out of solution. We model the foam as a system of identical spherical bubbles of gas, each surrounded by a layer of viscoelastic fluid containing a quantity of dissolved gas. The volume of this layer could be estimated by dividing the initial volume of liquid by the number of bubbles in the cured foam. We begin by describing general assumptions and follow this with a derivation of the governing equations. These are transformed into dimensionless form and we identify the relevant dimensionless groups.

We consider a spherical bubble of gas with an initial volume $(4/3)\pi u_0$, and gas pressure p_{g0} , expanding in a uniform spherical envelope of incompressible viscoelastic fluid that contains a limited supply of a dissolved ideal gas. Here, we are not attempting to model the initial rapid phase of bubble expansion immediately following nucleation, and so the initial bubble volume is not the volume at nucleation but a larger volume when the gas pressure is p_{g0} . Growth is driven by the pressure difference between the gas pressure inside the bubble, p_g , and a background pressure outside the envelope, p_a . We assume that the expansion rate is sufficiently small that fluid inertia may be neglected (see Section 2.2), bubble growth is isothermal, and the bubble–fluid interface remains in thermodynamic equilibrium.

2.1. Governing equations

In a spherically symmetric expansion, conservation of mass dictates that the radial velocity, q_r , of the fluid surrounding the bubble is given by

$$q_r = \frac{R^2 \dot{R}}{r^2},$$

where R is the bubble radius and r is the general radial position. The liquid surrounding the bubble is modelled as an Oldroyd-B fluid. There are three terms contributing to the stress, $\boldsymbol{\sigma}$, in the liquid: an isotropic pressure; a Newtonian viscous term with solvent viscosity μ ; and a polymer stress with elastic modulus G and orientation tensor \mathbf{A} :

$$\boldsymbol{\sigma} = -p\mathbf{I} + \mu(\nabla\mathbf{q} + \nabla\mathbf{q}^T) + G(\mathbf{A} - \mathbf{I}).$$

The orientation tensor satisfies

$$\overset{\nabla}{\mathbf{A}} = -\frac{1}{\tau}(\mathbf{A} - \mathbf{I}), \quad (1)$$

where $\overset{\nabla}{\mathbf{A}} = \partial\mathbf{A}/\partial t + \mathbf{q} \cdot \nabla\mathbf{A} - (\nabla\mathbf{q})^T \cdot \mathbf{A} - \mathbf{A} \cdot \nabla\mathbf{q}$ is the upper convected derivative and \mathbf{q} is the fluid velocity.

In spherical polar co-ordinates, $A_{\theta\theta} = A_{\phi\phi}$, and p , A_{rr} and $A_{\theta\theta}$ are assumed to depend on r and time t only. Neglecting inertia, the radial component of the momentum equation, $\nabla \cdot \boldsymbol{\sigma} = 0$, gives

$$0 = -\frac{\partial p}{\partial r} + \left(\frac{1}{r^2} \frac{\partial}{\partial r} \left(2\mu r^2 \frac{\partial q_r}{\partial r} \right) - \frac{4\mu q_r}{r^2} \right) + \left(\frac{1}{r^2} \frac{\partial}{\partial r} (r^2 G A_{rr}) - \frac{2G A_{\theta\theta}}{r} \right).$$

The term involving the Newtonian viscosity vanishes due to the spherical symmetry of the velocity field. Thus,

$$\frac{\partial p}{\partial r} = \frac{2G(A_{rr} - A_{\theta\theta})}{r} + G \frac{\partial A_{rr}}{\partial r}. \quad (2)$$

Since the fluid volume is conserved it is useful to transform from a radial co-ordinate r to a Lagrangian volume co-ordinate x such that $r^3 = u + x$. Here, $(4/3)\pi u$ is the bubble volume, $(4/3)\pi x$ is the general fluid volume and $(4/3)\pi X$ is the volume of fluid in the whole layer. Thus, $x = X$ is the Lagrangian position of the outer edge of the envelope. At the boundaries $x = 0$ and $x = X$

$$-p(u) - \frac{4\mu\dot{u}}{3u} + G A_{rr}(u) = -p_g + \frac{2S}{u^{1/3}}, \quad (\text{inner surface boundary condition})$$

$$-p(X + u) - \frac{4\mu\dot{u}}{3(X + u)} + G A_{rr}(X + u) = -p_a, \quad (\text{outer surface boundary condition})$$

where S is the surface tension at the bubble surface. Integrating Eq. (2) across the fluid layer and using these boundary conditions gives

$$\frac{4}{3}\mu\dot{u} \left[\frac{1}{u} - \frac{1}{X + u} \right] = p_g - p_a + \frac{2}{3}G \int_0^X \frac{A_{rr} - A_{\theta\theta}}{x + u} dx - \frac{2S}{u^{1/3}}. \quad (3)$$

Due to the co-ordinate transformation, the evolution of A_{rr} and $A_{\theta\theta}$, given by Eq. (1), can be followed in the Lagrangian frame:

$$\frac{\partial A_{rr}}{\partial t} = -\frac{4\dot{u}}{3(x + u)} A_{rr} - \frac{1}{\tau} (A_{rr} - 1), \quad (4)$$

$$\frac{\partial (A_{rr} - A_{\theta\theta})}{\partial t} = \frac{2\dot{u}}{3(x + u)} [(A_{rr} - A_{\theta\theta}) - 3A_{rr}] - \frac{1}{\tau} (A_{rr} - A_{\theta\theta}). \quad (5)$$

Initially, $A_{rr} = 1$ and $A_{rr} - A_{\theta\theta} = 0$ everywhere. The concentration of gas at the bubble surface ($x = 0$) is related to the pressure inside the bubble by Henry's law:

$$c(0, t) - c_0 = (p_g - p_{g0})H.$$

Here, c_0 is the initial gas concentration, p_{g0} is the initial gas pressure and H is the Henry's law constant. The concentration, $c(x, t)$, is the number of moles of gas per unit volume of fluid.

The gas diffusion equation is obtained via a mass balance in the fluid:

$$\frac{\partial c}{\partial t} = 9D \frac{\partial}{\partial x} \left((x+u)^{4/3} \frac{\partial c}{\partial x} \right).$$

We introduce a concentration potential $\phi(x, t)$ so that $\partial\phi/\partial x = c - c_0$ to aid in the numerical solution [1,3]. The diffusion equation then becomes

$$\frac{\partial\phi}{\partial t} = 9D(x+u)^{4/3} \frac{\partial^2\phi}{\partial x^2}, \quad (6)$$

with $\partial\phi/\partial x = (p_g - p_{g0})H$ at the bubble surface and $\partial^2\phi/\partial x^2 = 0$ at the outer edge of the fluid layer, which implies that ϕ is constant there. Thus, there is no gas transport through the outer edge of the fluid layer and gas supply is limited. Conservation of mass in the bubble gives

$$\frac{d}{dt} \left(\frac{p_g u}{RT} \right) = 9Du^{4/3} \frac{\partial^2\phi}{\partial x^2} \Big|_{x=0}.$$

Substituting from Eq. (6) and integrating with respect to time gives

$$p_g u = p_{g0} u_0 + RT\phi(0, t), \quad (7)$$

since we can arbitrarily set $\phi(0, 0) = 0$. Here, R and T are, respectively, the gas constant and temperature.

Eqs. (3)–(7) together with initial conditions $A_{rr} = 1$ and $A_{rr} - A_{\theta\theta} = 0$, $u = u_0$ and $p_g = p_{g0}$ govern bubble growth.

2.2. Non-dimensional equations

We scale all lengths with the initial bubble radius $u_0^{1/3}$ and scale times with the polymer relaxation time τ . Pressure is scaled so that the dimensionless gas pressure, P_g , is the ratio of the current pressure difference to the initial pressure difference: i.e. $P_g = (p_g - p_a)/(p_{g0} - p_a)$. The number of moles of gas which have diffused out of the liquid, ϕ , is scaled with the initial number of moles of gas in the bubble, $p_{g0}u_0/RT$, giving the following dimensionless equations:

$$\frac{4}{3}\dot{u} \left[\frac{1}{u} - \frac{1}{X+u} \right] = P_g De + \frac{2}{3}\gamma \int_0^X \frac{A_{rr} - A_{\theta\theta}}{x+u} dx - \frac{1}{\Gamma u^{1/3}}, \quad (8)$$

$$\frac{\partial A_{rr}}{\partial t} = -\frac{4\dot{u}}{3(x+u)} A_{rr} - (A_{rr} - 1), \quad (9)$$

$$\frac{\partial(A_{rr} - A_{\theta\theta})}{\partial t} = \frac{2\dot{u}}{3(x+u)} [(A_{rr} - A_{\theta\theta}) - 3A_{rr}] - (A_{rr} - A_{\theta\theta}), \quad (10)$$

$$\left(\frac{p_a + (p_{g0} - p_a)P_g}{p_{g0}} \right) u = 1 + \phi(0, t), \quad (11)$$

$$\frac{\partial\phi}{\partial t} = N(x+u)^{4/3} \frac{\partial^2\phi}{\partial x^2}, \quad (12)$$

Table 1

Dimensionless groups arising in the non-dimensional formulation of the equations governing bubble growth

Deborah number	$De = \frac{(p_{g0} - p_a)\tau}{\mu}$	Ratio of the rate of bubble growth in the solvent to the relaxation rate of the polymer
Viscosity ratio	$\gamma = \frac{G\tau}{\mu}$	Ratio of polymer to solvent contributions to the steady shear viscosity
Capillary number	$\Gamma = \frac{u_0^{1/3}\mu}{2S\tau}$	Ratio of viscous force to surface tension
Timescale ratio	$N = \frac{9D\tau}{u_0^{2/3}} = \frac{\tau}{T_d}$ $\Phi = RTH$	Ratio of the polymer relaxation time, τ , to gas diffusion time, T_d

together with boundary conditions:

$$\frac{\partial\phi}{\partial x} = \Phi \frac{p_{g0} - p_a}{p_{g0}} (P_g - 1) \quad (\text{at the bubble surface, } x = 0)$$

$$\frac{\partial^2\phi}{\partial x^2} = 0 \quad (\text{at } x = X)$$
(13)

and initial conditions $A_{rr} = 1$ and $A_{rr} - A_{\theta\theta} = 0$, $u = 1$ and $P_g = 1$. The five non-dimensional groups we use are described in Table 1. Eqs. (8)–(12) were solved using an Euler method with an adaptive time step for Eqs. (8)–(10) and a Crank–Nicolson method for the diffusion equation. The parameter values and values of the dimensionless groups used are shown in Tables 2 and 3, respectively. The initial concentration of gas in the liquid is, by Henry's law, 105 mol m^{-3} . With a liquid density of 1200 kg m^{-3} and molar mass of $0.044 \text{ kg mol}^{-1}$ for carbon dioxide this corresponds to an initial gas concentration of 0.385%. Henry's law is valid for dilute solutions where gas concentrations are of the order of 1%.

In order to neglect inertia from this model, the Reynolds number for the bubble expansion must be small. Balancing the inertia term with the viscosity term in the momentum equation gives a Reynolds number

$$Re = \frac{\rho u_0^{2/3} (p_{g0} - p_a)}{\mu^2}$$

Table 2

Parameters required for bubble expansion driven by gas diffusion

Parameter	Value	Units
Pressure outside the fluid layer, p_a	1	10^5 N m^{-2}
Initial bubble gas pressure, p_{g0}	10	10^5 N m^{-2}
Elastic modulus, G	1–10	10^5 N m^{-2}
Solvent viscosity, μ	1, 6	10^5 N s m^{-2}
Polymer relaxation time, τ	1	s
Initial bubble volume, u_0	1	10^{-18} m^3
Surface tension, S	0–5	10^{-1} N m^{-1}
Gas constant, R	8.3	$\text{J mol}^{-1} \text{ K}^{-1}$
Temperature, T	370	K
Henry's law constant, H	10.5	$10^{-5} \text{ mol N}^{-1} \text{ m}^{-1}$
Diffusivity, D	0.1– ∞	$10^{-12} \text{ m}^2 \text{ s}^{-1}$
Fluid density, ρ	1200	kg m^{-3}

Table 3
Dimensionless numbers used for bubble expansion driven by gas diffusion

Dimensionless groups	Value
De	9–1.5
γ	1–10
Γ	0.1– ∞
N	0.9– ∞
Φ	0.32
X	53.6

(using τ/De as the timescale for the bubble expansion). With the parameter values given in Table 2, the Reynolds number for the bubble expansion is 1.08×10^{-13} .

2.3. Results and discussion

In this problem, there are three distinct timescales controlling the expansion of the bubble. These are the diffusion time for gas transport into the bubble from the surrounding fluid; the viscous growth time for a bubble in a viscous fluid of the solvent viscosity; and the relaxation time of the polymer, τ . From Eq. (12), the timescale for gas to diffuse across the fluid layer is of the order $(u_0 X)^{2/3}/9D = X^{2/3}\tau/N$, while the solvent viscosity imposes a maximum bubble expansion rate of order $(p_{g0} - p_a)/\mu = De/\tau$. Depending upon the relative values of these timescales bubble growth may be controlled by any one of these three timescales. We can examine the effects of viscoelasticity on growth rate by considering the limit $N \gg DeX^{2/3}$ when diffusion is, essentially, instantaneous so that the bubble growth is limited by the rheology of the surrounding fluid. In this case, the concentration profile of gas in the liquid is independent of fluid volume and is dictated by the gas pressure in the bubble through Henry's law. Now Eq. (13) applies throughout the fluid layer and the conservation of mass equation (Eq. (11)) becomes

$$\left(\frac{p_a + (p_{g0} - p_a)P_g}{p_{g0}} \right) u = 1 + \Phi \frac{p_{g0} - p_a}{p_{g0}} (1 - P_g) X.$$

This enables the bubble growth equations to be solved independently of the diffusion equation. In the case when ΦX is large so that there is large reservoir of gas available within the layer, the gas pressure P_g remains approximately constant until $u \simeq \Phi X$ after which the pressure difference decays to zero in the absence of surface tension. In the opposite limit when $\Phi X \ll 1$ and $p_{g0} \gg p_a$ so that most of the gas is already within the bubble at $t = 0$ the pressure decreases as $1/u$.

In Fig. 1, we compare the growth rate of bubbles at different Deborah numbers for the same value of γ . At large Deborah numbers, we see two distinct phases of bubble growth: an initial rapid expansion in which the bubble volume increases rapidly, and a slower second phase of expansion. As the polymers are initially unstretched they do not provide any resistance during the initial phase of expansion, so that the resistance comes only from the solvent viscosity. The rapid expansion during this phase causes the polymer to stretch so that $A_{\theta\theta} - A_{rr}$ increases (see Fig. 2). This phase of expansion stops once the normal stress difference $\gamma(A_{\theta\theta} - A_{rr})/De$ at the surface of the bubble becomes comparable to the pressure difference. During the second phase the pressure difference is balanced by the elastic normal stress difference within

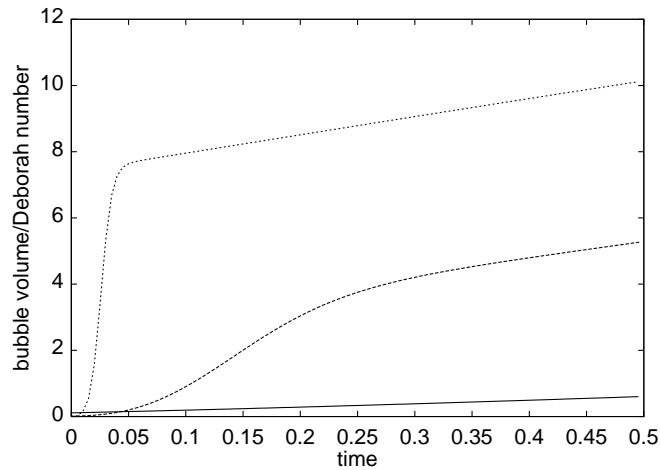


Fig. 1. Effect of viscoelasticity on bubble volume when $\gamma = 5$. Solid line: $De = 9$; long dashed line: $De = 99$; short dashed line: $De = 999$.

the fluid. The growth of the bubble is therefore controlled by the relaxation of the elastic stress, which relaxes on a timescale of order τ , the unit of time in our non-dimensionalisation.

We can attempt to estimate the timescales for the first phase in the two limits described above of large and small ΦX . If Γ and X are both large and polymer does not contribute to the stress then Eq. (8) may be approximated as

$$\frac{\dot{u}}{u} = \frac{3}{4} P_g De.$$

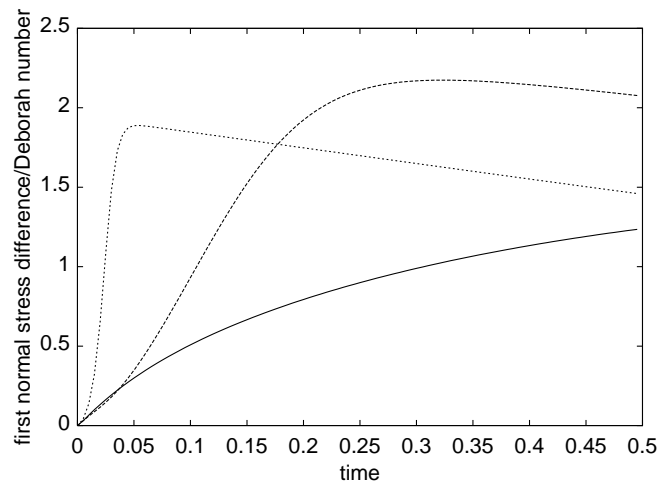


Fig. 2. Effect of viscoelasticity on the first normal stress difference when $\gamma = 5$. Solid line: $De = 9$; long dashed line: $De = 99$; short dashed line: $De = 999$.

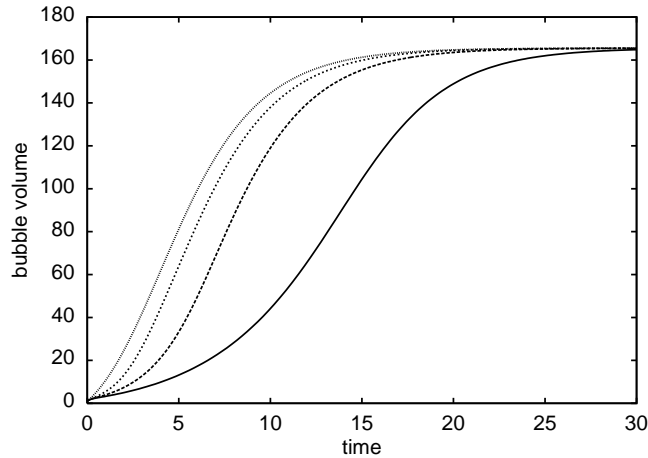


Fig. 3. Effect of diffusivity on bubble growth rate when $\gamma = 5$. Solid line: $N = 0.9$; long dashed line: $N = 4.5$; short dashed line: $N = 18$; dotted line is the limit $N \rightarrow \infty$.

As the bubble grows $A_{\theta\theta}$ increases while A_{rr} decreases so that, neglecting A_{rr} in Eq. (10), the polymer stretch difference on the bubble surface evolves approximately as

$$\frac{\partial(A_{\theta\theta} - A_{rr})}{\partial t} = \left(\frac{2\dot{u}}{3u} - 1 \right) (A_{\theta\theta} - A_{rr}).$$

Using these approximate equations we find, for ΦX large, that the bubble volume increases exponentially as approximately $\exp(3Det/4)$ and $A_{\theta\theta} - A_{rr} \simeq \exp\{((1/2)De - 1)t\}$. Thus, the elastic stress will balance the pressure difference after a time of order $2/(De - 2) \log\{(De/\gamma)\}$. In the opposite limit, the bubble volume grows linearly as approximately $1 + 3Det/4$, while $A_{\theta\theta} - A_{rr}$ increases as $u^{2/3} \exp(-t)$. The elastic stress will now balance the pressure difference when $(1 + (3/4)Det) \exp(-3t/5) = (De/\gamma)^{3/5}$, so that for large De this will be at a time of order $De^{-2/5} \gamma^{-3/5}$. In practice, it is difficult to see these scalings as rather extreme values of the parameters are required to make the approximations accurate.

When $N \ll DeX^{2/3}$ bubble growth is limited by diffusion rather than rheology. (In fact, since De is an overestimate of the bubble growth rate, this limit applies at $N \approx DeX^{2/3}$.) Growth is slow initially as the bubble has a small surface area over which the gas can diffuse (see Fig. 3). The expansion rate increases as the bubble gets larger but subsequently decreases once the gas pressure approaches the pressure outside the fluid layer and the concentration of gas in the liquid reaches a uniform profile. In the initial phase of expansion the pressure drops rapidly inside the bubble as it expands. The polymer stress builds to a maximum and then decays as the expansion rate decreases. However, the stress is prevented from relaxing completely by gas diffusing into the bubble. Between $t = 5$ and 15, we see a plateau in the first normal stress difference and a decrease in the rate of pressure drop (see Figs. 4 and 5, $N = 0.9$ curve) corresponding to an increase in gas transport into the bubble. The stress is finally allowed to relax once the gas concentration in the bulk falls.

As diffusivity is increased the pattern of bubble growth remains qualitatively similar, but with an increase in the bubble growth rate. Increased diffusion reduces the extent of the initial rapid pressure drop until, in the limit of infinite diffusion, this initial phase is lost altogether (see Fig. 4). Increasing diffusion

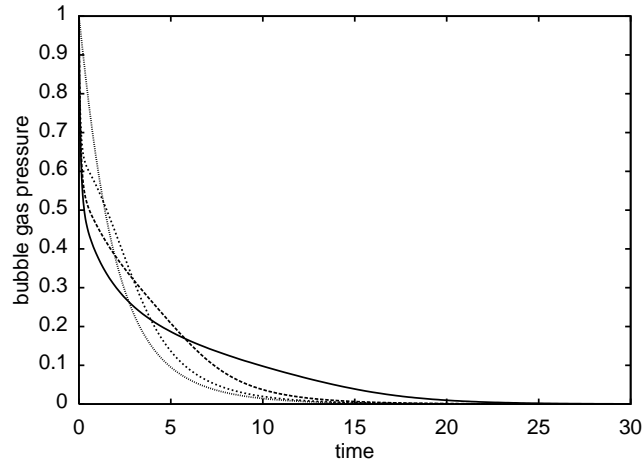


Fig. 4. Effect of diffusivity on dimensionless gas pressure (ratio of the pressure difference to the initial pressure difference) when $\gamma = 5$. Solid line: $N = 0.9$; long dashed line: $N = 4.5$; short dashed line: $N = 18$; dotted line is the limit $N \rightarrow \infty$.

also causes the final stress relaxation to occur sooner and the more rapid bubble growth increases the magnitude of the first normal stress difference at its peak. These two regions eventually become indistinct (Fig. 5).

The parameter γ is the ratio of the polymer to solvent contributions to the zero shear-rate viscosity with $\gamma = 0$ corresponding to a Newtonian fluid and $\gamma = \infty$ to an upper convected Maxwell fluid. Initially, the polymers are unstretched and so the first stage of bubble growth is resisted only by the solvent stress. Consequently, bubbles grow more rapidly in a viscoelastic liquid than in a Newtonian fluid of the same zero shear-rate viscosity. This is shown in Fig. 6, where we compare growth in fluids with the same zero shear-rate viscosity at $N = 0.9$ and in the limit of infinite diffusivity. The difference in growth

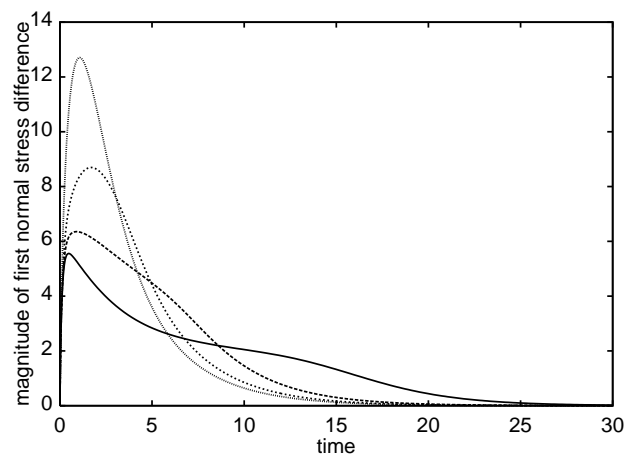


Fig. 5. Effect of diffusivity on the magnitude of the first normal stress difference, $\gamma|A_{rr} - A_{\theta\theta}|$, at the bubble surface when $\gamma = 5$. Solid line: $N = 0.9$; long dashed line: $N = 4.5$; short dashed line: $N = 18$; dotted line is the limit $N \rightarrow \infty$.

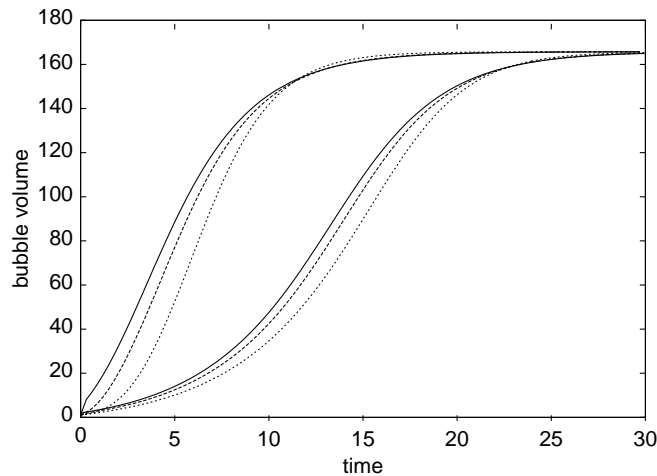


Fig. 6. Comparison of bubble growth in a viscoelastic liquid and a Newtonian liquid of the same zero shear-rate viscosity. The solid lines represent a viscoelastic liquid with $\gamma = \infty$ and $De = 9$, the long dashed lines represent a viscoelastic liquid with $\gamma = 4$ and $\mu = 2$, and the short dashed line represents a Newtonian liquid with $\gamma = 0$. The lower curves show bubble growth rate when $N = 0.9$ and the upper curves show bubble growth rate in the limit of infinite diffusion.

rate is most marked at high diffusivity where the initial growth rate is controlled by the fluid viscosity. At low diffusivity viscoelastic effects are less significant due to slower growth rate. The calculations of Arafmanesh and Advani [2] correspond to the limit $\gamma \rightarrow \infty$. As they did not include a solvent term they were forced to use an iterative technique to obtain solutions. However, by taking large values of γ we are able to reproduce their results.

The potential, ϕ , is the relative number of moles of gas diffused from the liquid at time t . In the absence of surface tension, as $t \rightarrow \infty$, the dimensionless gas pressure $P_g \rightarrow 0$ and $\phi \rightarrow \Phi(p_{g0} - p_a)X/p_{g0}$. This

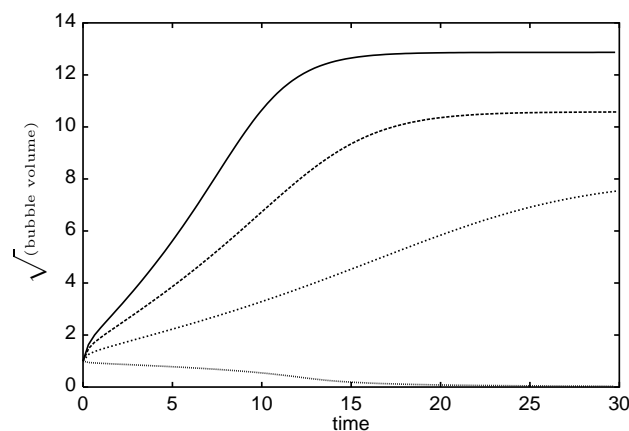


Fig. 7. Effect of surface tension ($\Gamma < \infty$) on bubble growth rate, $N = 0.9$, $De = 9$ and $\gamma = 5$. The solid line shows $\Gamma = \infty$; the two lines with positive bubble growth rate ($\Gamma > 1/De$) show successively smaller equilibrium bubble volumes with $\Gamma = 0.5$ and $\Gamma = 0.2$, respectively. The line with negative bubble growth rate shows $\Gamma = 0.1 < 1/De$.

leads to an equilibrium bubble volume given by

$$u_{\infty} = \frac{p_{g0} + \Phi(p_{g0} - p_a)X}{p_a}.$$

Nucleation and the early stages of bubble growth involve a period of surface tension dominated growth or collapse. In this paper, we assume that the initial bubble volume is large enough that $\Gamma > 1/De$. In this case, surface tension again dominates the bubble growth rate towards the end of the expansion as $P_g De - 1/\Gamma u^{1/3} \rightarrow 0$. Thus, the effect of including surface tension at the bubble surface ($\Gamma < \infty$) is to increase the equilibrium gas pressure and reduce the equilibrium bubble volume, see Fig. 7.

3. Bubble growth in a reacting polymer

In order to describe bubble growth in a reacting polymer, the model of the previous section must be modified in two respects. First, we must account for the production of gas as a by-product of the reaction. Second, we require a constitutive model that accounts for the increase in molecular weight of the polymer as the reaction proceeds. For simplicity, we assume that the polymer is formed from a single reacting species. The reactant forms self-similar molecules of increasing molecular weight that ultimately form a gel.

3.1. Reaction kinetics

We assume that the reaction follows second order kinetics so that the extent of reaction, α , is given by

$$\frac{d\alpha}{dt} = c_{\alpha}(1 - \alpha)^2, \quad (14)$$

where α is the fraction of reacted end groups at time t and c_{α} is the reaction rate. We now scale time with the reaction rate, c_{α} , so that in dimensionless units as the relaxation time of the fluid varies with time,

$$\frac{d\alpha}{dt} = (1 - \alpha)^2. \quad (15)$$

We assume that gas is generated at a rate proportional to $d\alpha/dt$. The concentration of gas generated at time t is $\zeta H p_a (\alpha - \alpha_0)$, where α_0 is the extent of reaction at nucleation, and ζ is a dimensionless parameter giving the number of moles of dissolved gas per unit volume generated by the reaction at completion. In order to satisfy Henry's law at the bubble surface $p_{g0} = p_a(1 + \zeta\alpha_0)$ initially. We now scale ϕ with the maximum number of moles of gas produced by the reaction, $\zeta H p_a X$, so that the diffusion equation (Eq. (12)) becomes

$$\frac{\partial \phi}{\partial t} = N(x + u)^{4/3} \frac{\partial^2 \phi}{\partial x^2} - \frac{1}{X} \frac{d\alpha}{dt} (X - x). \quad (16)$$

The boundary condition (13) is

$$\frac{\partial \phi}{\partial x} = \frac{1}{\zeta X} \frac{p_{g0} - p_a}{p_a} (P_g - 1) \quad (17)$$

at the bubble surface and $\partial^2 \phi / \partial x^2 = 0$ at $x = X$. The dimensionless group $N = 9D/u_0^{2/3} c_{\alpha}$ is now the ratio of the gas diffusion rate to the reaction rate.

The conservation of mass equation (Eq. (11)), becomes

$$\left(\frac{p_a + (p_{g0} - p_a)P_g}{p_{g0}} \right) u = 1 + \zeta \Phi \frac{p_a}{p_{g0}} X(\phi(0, t) + (\alpha - \alpha_0)). \quad (18)$$

3.2. Rheological model

Our rheological model for the reacting polymer is based on the dynamic scaling model of Rubinstein et al. [14] for the linear rheology of a gelling fluid.

We assume that the polymer molecules in the fluid surrounding the bubble begin as self-similar chains with molecular weight m_x and slowest relaxation rate ϵ_x . All relaxation processes faster than ϵ_x will be incorporated into a background solvent viscosity. We also assume that the polymer solution is semi-dilute so that the polymer molecules are close enough to screen hydrodynamic interactions, but are not entangled.

The molecules start to react and bond to form molecules with a range of molecular weights, each with a Rouse spectrum of relaxation modes [5] approximated as a continuous spectrum $\epsilon(k)$, so that the relaxation modulus $G_m(t)$ for molecules of mass m is given by

$$G_m(t) = \frac{\rho_m RT}{m} \int_1^{m/m_x} e^{-\epsilon_m(k)t} dk, \quad (19)$$

where k is the mode number which runs from 1 (the slowest mode) to m/m_x , the number of segments of molecular weight m_x . Here, ρ_m , R and T are, respectively, the density of molecules of mass m , gas constant and temperature. In Rouse dynamics, the friction on a molecular segment is proportional to the number of monomers so that the diffusion coefficient is inversely proportional to molecular weight. The longest relaxation time for a molecule of molecular mass m and radius of gyration r will, therefore, scale as $\epsilon_m \propto 1/mr^2$. The radius of gyration, r , increases as m^{1/d_f} , where d_f is the fractal dimension of the equilibrium coil size. Hence, the longest relaxation rate, ϵ_m , satisfies

$$\frac{\epsilon_m}{\epsilon_x} = \left(\frac{m}{m_x} \right)^{-((2/d_f)+1)}.$$

The k th mode corresponds to the relaxation of sections of mass $m/m_x k$, hence from this scaling argument, we obtain the relaxation rate, ϵ , for mode k as

$$\epsilon = \epsilon_m(k) = \epsilon_x \left(\frac{m_x k}{m} \right)^{((2/d_f)+1)}.$$

Changing the variable of integration from k to ϵ in Eq. (19) gives the result of Rubinstein et al. [14]:

$$G_m(t) = mn(m) \frac{d_r}{2} G_0 \int_{\epsilon_m}^{\epsilon_x} \left(\frac{\epsilon}{\epsilon_x} \right)^{d_f/2} e^{-\epsilon t} \frac{d\epsilon}{\epsilon}. \quad (20)$$

Here, $2/d_r = 1 + 2/d_f$, $G_0 = \rho RT/m_x$, and $mn(m) = \rho_m/\rho$ is the number density of molecules of molecular weight m . We assume that the number density $n(m)$ follows a power law between the minimum and maximum molecular weights m_x and m_{ch} so that $n(m) \propto m^{-\nu}$. The value of ν close to the gel point can be obtained from percolation theory [17] or by Monte Carlo simulations [6]. It has been shown [6,11] that the value of ν obtained by Monte Carlo simulations provides an accurate description near the gel point. For simplicity in our simulations, we use this value of $\nu = 2.2$ throughout the reaction

though one could use the value of $\nu = 2.5$ from mean field theory [17] to improve accuracy further from the gel point. Following Rubinstein et al. [14], we impose a step cut-off at the minimum and maximum molecular weights so that prior to the gel point α_c

$$n(m) = \frac{(\nu - 2)m_x^{\nu-2}}{1 - (m_x/m_{ch})^{\nu-2}} m^{-\nu}, \quad \alpha < \alpha_c; \quad m_x < m < m_{ch},$$

$$n(m) = 0, \quad \alpha < \alpha_c; \quad m > m_{ch}; \quad m < m_x.$$

Randrianantoandro et al. [13] use Monte Carlo simulations to obtain a more accurate exponential cut-off function that is in good agreement with experimental data [6]. However, for the sake of simplicity we retain the step function cut-off.

Integrating Eq. (20) over all molecular weights from m_x to m_{ch} gives the relaxation modulus prior to gelation ($\alpha < \alpha_c$) as

$$G(t) = \frac{G_0(d_r/2)}{1 - (\epsilon_{ch}/\epsilon_x)^{(1/2)d_r(\nu-2)}} \int_{\epsilon_{ch}}^{\epsilon_x} \left(\left(\frac{\epsilon}{\epsilon_x} \right)^{(1/2)d_r(\nu-1)} - \left(\frac{\epsilon_{ch}}{\epsilon_x} \right)^{(1/2)d_r(\nu-2)} \left(\frac{\epsilon}{\epsilon_x} \right)^{d_r/2} \right) e^{-\epsilon t} \frac{d\epsilon}{\epsilon}. \quad (21)$$

Beyond the gel point, the largest molecular weight is infinite and we use m_{ch} to denote the molecular weight of the largest free molecule. We assume that the only reactions are between the longest molecules in the solution and the gel so that the number density is now

$$n(m) = (\nu - 2)m_x^{\nu-2} m^{-\nu}, \quad \alpha > \alpha_c; \quad m_x < m < m_{ch}.$$

The relaxation modulus of the free molecules is still given by Eq. (20) so that integrating over molecular weights from m_x to m_{ch} and changing the order of integration gives

$$G(t)_{\text{sol}} = G_0 \frac{d_r}{2} \int_{\epsilon_{ch}}^{\epsilon_x} \int_{m_\epsilon}^{m_{ch}} mn(m) \left(\frac{\epsilon}{\epsilon_x} \right)^{(1/2)d_r} \frac{e^{-\epsilon t}}{\epsilon} dm d\epsilon.$$

For the remaining $(m_x/m_{ch})^{\nu-2}$ fraction making up the gel, we assume that only modes faster than ϵ_{ch} can relax (the first term) with the remainder making up the elastic modulus

$$G(t)_{\text{gel}} = G_0 \left(\frac{m_x}{m_{ch}} \right)^{\nu-2} \frac{d_r}{2} \left(\int_{\epsilon_{ch}}^{\epsilon_x} \left(\frac{\epsilon}{\epsilon_x} \right)^{(1/2)d_r} e^{-\epsilon t} \frac{d\epsilon}{\epsilon} \right) + G_0 \left(\frac{m_x}{m_{ch}} \right)^{\nu-1}.$$

Combining the contributions from both the sol fraction and the gel we obtain

$$G(t) = G_0 \frac{d_r}{2} \left(\int_{\epsilon_{ch}}^{\epsilon_x} \left(\frac{\epsilon}{\epsilon_x} \right)^{(1/2)d_r(\nu-1)} e^{-\epsilon t} \frac{d\epsilon}{\epsilon} \right) + G_0 \left(\frac{\epsilon_{ch}}{\epsilon_x} \right)^{(1/2)d_r(\nu-1)}. \quad (22)$$

Having obtained the relaxation modulus we now discretise the linear spectrum into a set of discrete modes

$$G(t) = \sum G_i e^{-\epsilon_i t}.$$

In order to extend this to non-linear flows, each mode is treated as a mode in a multimode Oldroyd-B fluid. This simple non-linear extension does not introduce any additional parameters. This extension will

be valid provided that molecular strains remain modest so that molecular segments do not extend beyond their maximum length.

For $\alpha < \alpha_c$, we use Eq. (21) to obtain G_i . A_{rr} and $A_{rr} - A_{\theta\theta}$ for each mode satisfy

$$\frac{\partial A_{rr}}{\partial t} = -\frac{4\dot{u}}{3(x+u)}A_{rr} - \frac{\epsilon}{c_\alpha}(A_{rr} - 1) \quad (23)$$

and

$$\frac{\partial(A_{rr} - A_{\theta\theta})}{\partial t} = \frac{2\dot{u}}{3(x+u)}[(A_{rr} - A_{\theta\theta}) - 3A_{rr}] - \frac{\epsilon}{c_\alpha}(A_{rr} - A_{\theta\theta}). \quad (24)$$

The values of the elastic moduli change during the reaction due to the loss of translational modes and the subsequent gain of internal modes. In addition new modes are ‘switched on’ as larger molecules are produced. This means that in order to conserve stress we must adjust \mathbf{A} for each mode so that when G changes by an amount ΔG ,

$$(G + \Delta G)\mathbf{A}_{\text{new}} = G\mathbf{A} + \Delta G\mathbf{I}. \quad (25)$$

Finally, we sum the modes in the momentum equation (Eq. (8)):

$$\frac{4}{3}\dot{u}\left[\frac{1}{u} - \frac{1}{X+u}\right] = P_g M + \frac{2}{3}\gamma \sum_{\epsilon=\epsilon_{\text{ch}}}^{\epsilon_x} G \int_0^X \frac{(A_{rr} - A_{\theta\theta})}{x+u} dx d(\ln \epsilon) - \frac{1}{\Gamma u^{1/3}}. \quad (26)$$

Here, $M = (p_{g0} - p_a)/\mu c_\alpha$ is the ratio of the bubble growth rate in the solvent to the reaction rate, $\gamma = G_0/\mu c_\alpha$ and $\Gamma = u_0^{1/3} \mu c_\alpha / 2S$.

For $\alpha > \alpha_c$, a gel is formed resulting in an additional mode corresponding to an elastic solid. This mode has modulus G_{gel} given by the second term in Eq. (22), and an infinite relaxation time. The increase in modulus of this mode with extent of reaction can be attributed to three sources: first from the translational modes of molecules attaching to the gel; second from modes near ϵ_{ch} in these molecules, which are frozen as they attach to the gel; and third from modes already in the gel which become frozen as ϵ_{ch} changes. Hence, as α increases and ϵ_{ch} decreases past the gel point, all modes with $\epsilon > \epsilon_{\text{ch}}$ are switched off. Both their modulus ΔG_{off} and their stress $\Delta G_{\text{off}}\mathbf{A}_{\text{off}}$ are added to the gel mode accounting for contributions two and three above. The contribution from the translational modes corresponds to an additional contribution $\Delta G_{\text{gel}}\mathbf{I}$. Thus, for the gel mode,

$$(G_{\text{gel}} + \Delta G_{\text{gel}} + \Delta G_{\text{off}})\mathbf{A}_{\text{new}} = G_{\text{gel}}\mathbf{A} + \Delta G_{\text{gel}}\mathbf{I} + \Delta G_{\text{off}}\mathbf{A}_{\text{off}}.$$

To complete our formulation we must relate the characteristic relaxation rate, ϵ_{ch} , to the extent of reaction α . Near the gel point, α_c , the largest molecular weight $m_{\text{ch}} \sim (\alpha - \alpha_c)^{-1/\sigma}$ [14]. Therefore, the slowest relaxation rate $\epsilon_{\text{ch}} \sim (\alpha - \alpha_c)^{2/\sigma d_r}$. The value of σ can be obtained from percolation theory [17] or by Monte Carlo simulations [6] and we use the value of 0.45 obtained by Monte Carlo simulations. In our model, we assume that this scaling applies throughout the reaction. Since the reaction begins with all the molecules having the same molecular weight, m_x , before the gel point we have

$$\epsilon_{\text{ch}} = \epsilon_x \left(\frac{\alpha_c - \alpha}{\alpha_c} \right)^{2/\sigma d_r}. \quad (27)$$

Randrianantoandro et al. [13] used Monte Carlo simulations to determine the prefactors before and after the gel point for their parameter $|(\alpha - \alpha_c)/\alpha_c|$ which scales with $m_z^{-\sigma}$. From the ratio of these prefactors, we can determine the scaling for ϵ_{ch} with α after the gel point

$$\epsilon_{\text{ch}} = \beta \epsilon_x \left(\frac{\alpha - \alpha_c}{\alpha_c} \right)^{2/\sigma d_t}, \quad (28)$$

where $\beta = 0.0049$. A value of β greater than

$$\left(\frac{\alpha_c}{1 - \alpha_c} \right)^{2/\sigma d_t}$$

allows for the fact that the network may not be an exactly self similar structure and may have ‘dangling arm’ sections with $\epsilon < \epsilon_x$ which are able to relax [13]. In our simulations, we choose $\beta = (\alpha_c/(1 - \alpha_c))^{2/\sigma d_t}$ for the sake of simplicity.

Eq. (15) for the reaction rate; Eq. (16) for gas diffusion; Eq. (18) for bubble gas pressure; Eqs. (23)–(25) for the elastic stresses; Eq. (26) for the bubble growth rate; and Eqs. (27) and (28) for the evolution of the shortest relaxation rate provide a dimensionless equation set governing bubble growth in a gelling system. Here, time is scaled with the reaction time, ϕ with the maximum number of moles of gas produced by the reaction and bubble gas pressure and lengths are scaled as in Section 2.2. The method of solution is that described in Section 2.3. Numerically, 20 modes per decade give a sufficiently accurate description of the viscoelastic spectrum.

3.3. Linear viscoelastic response

In this section, we show the model’s predictions for the viscosity, gel modulus and response to step-strain. Table 4 lists the parameter values used in addition to those given in Tables 2 and 5 summarises the dimensionless groups arising and their values.

Fig. 8 shows the steady viscosity of the sol fraction, and the elastic modulus of the gel, with reaction extent. Here, viscosity is scaled with the steady viscosity of the polymer at $\alpha = 0$, G_0/ϵ_x , and the elastic modulus is scaled with the elastic modulus of the fully developed gel, G_0 . At the gel point, the steady

Table 4
Additional parameters required for bubble expansion in a reacting polymer

Parameter	Value	Units
Molar mass of initial polymers, m_x	0.5	kg mol ⁻¹
Relaxation rate of initial polymers, ϵ_x	750	s ⁻¹
Liquid density, ρ	1200	kg m ⁻³
Rate of reaction, c_α	1, 10	s ⁻¹
Maximum gas concentration produced by reaction/background gas concentration, ζ	10	–
Extent of reaction at the gel point, α_c	0.91	–
Extent of reaction at nucleation, α_0	0.1	–
Molecular weight distribution exponent, ν	2.2	–
Largest molecular weight scaling exponent, σ	0.45	–
Fractal dimension of the equilibrium coil size of a molecule, d_t	2.5	–
Solvent viscosity, μ	0.1	10 ⁵ N s m ⁻²

Table 5

Dimensionless groups arising in the non-dimensional formulation of the equations governing bubble growth in a gelling system

$M = \frac{P_{g0} - P_a}{\mu c_\alpha}$	1, 10	Ratio of the rate of bubble growth in the solvent to the reaction rate
$\gamma = \frac{G_0}{\mu c_\alpha}$	73.8, 738	
$\Gamma = \frac{u_0^1/3\mu c_\alpha}{2S}$	∞	Ratio of viscous force to surface tension
$N = \frac{9D}{u_0^{1/3} c_\alpha}$	$0.9 \rightarrow \infty$	Ratio of the rate of gas diffusion to the reaction rate
$\Phi = RTH$	0.32	
X	53.6	Dimensionless fluid volume

viscosity diverges and we see the development of the elastic modulus. Near the gel point, the viscosity scales with

$$(\alpha_c - \alpha)^{(2/\sigma d_r) - (v-1)/\sigma}$$

and the elastic modulus scales with

$$(\alpha - \alpha_c)^{(v-1)/\sigma}.$$

Figs. 9 and 10 show the response of the fluid to small amplitude oscillations of frequency ω . The storage modulus $G'(\omega)$ increases with α and we see a change from a gradient of two corresponding to a single relaxation mode to a gradient of $d_r(v - 1)/2 = 0.666$ at the gel point. Below the gel point we see a transition from a gradient of two for frequencies below ϵ_{ch} to a gradient of 0.666 at higher frequencies. Beyond the gel point, G' tends to the elastic modulus of the gel fraction at low frequencies. The loss modulus, $G''(\omega)$, at first increases with α up to the gel point as the molecular weight increases. However,

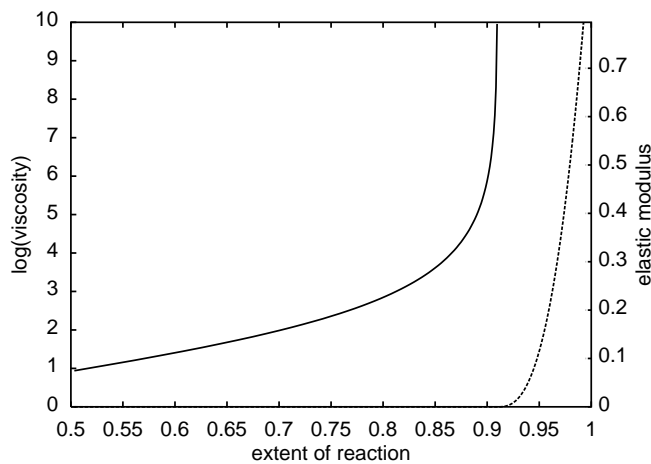


Fig. 8. Viscosity relative to the viscosity at $\alpha = 0$ in the sol phase (solid line) and elastic modulus relative to the elastic modulus of the fully developed gel in the gel phase (broken line).

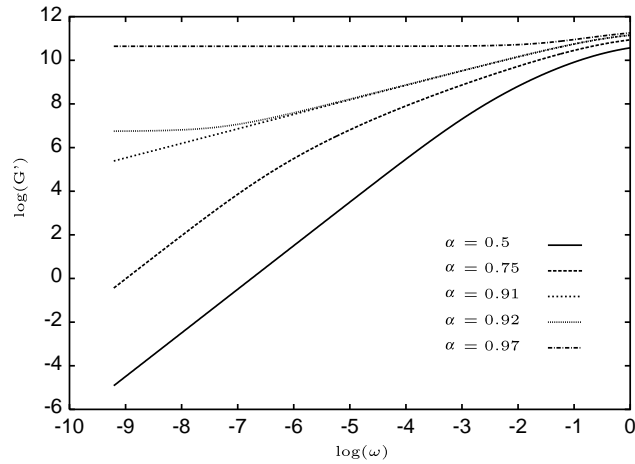


Fig. 9. Storage modulus, $G'(\omega)$, at various extents of reaction.

beyond the gel point, it decreases again as higher molecular weight material becomes part of the gel. Again we see a change in gradient from unity at frequencies below ϵ_{ch} to 0.666 at higher frequencies.

Our model gives qualitatively similar results to those of Randrianantoandro et al. [13]. At high frequencies, their model shows a further change in gradient due to the α -relaxation in the low molecular weight segments which we incorporate into an effective viscosity. Their model also predicts an undershoot in G' after the gel point caused by the difference in the form of the high molecular weight cut off function.

3.4. Effects on bubble growth

We now consider the growth rate of a bubble in a reacting polymer in which gas is produced as a reaction by-product.

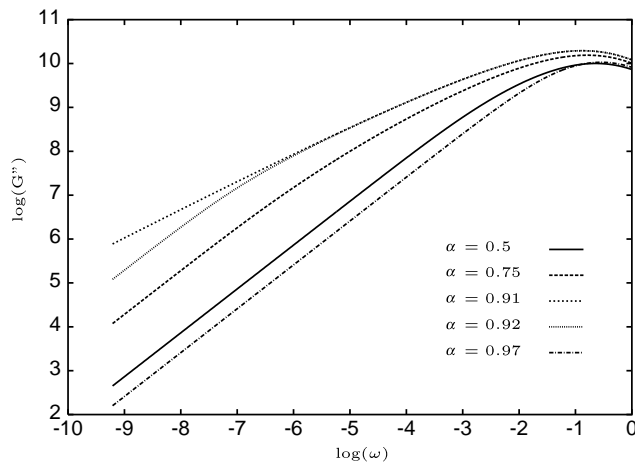


Fig. 10. Loss modulus, $G''(\omega)$, at various extents of reaction.

As in the non-reacting model, the rate of diffusion of gas is of order

$$\frac{9D}{(u_0 X)^{2/3}}$$

while the maximum bubble expansion rate is of order

$$\frac{Sp_a}{\mu}.$$

There is now a third timescale, the reaction rate c_α , which determines both the production of gas and the evolution of the fluid rheology. Here, we describe how the balance of these timescales controls bubble growth dynamics. For simplicity we have assumed that the gas diffusivity, D , is independent of the extent of reaction. Although there will be a change in diffusivity between the initial and final states of the material, most of the gas is produced in the early stages of the reaction and in most cases diffusion takes place well before the gel point.

The initial phase of bubble growth is controlled by supply of gas into the bubble. There are now two distinct sources of gas available to drive bubble growth. First, some gas is present in the liquid initially and will immediately begin to diffuse into the bubble. Second, gas will be produced within the liquid as the reaction progresses and, if the production rate exceeds the rate of transport into the bubble, the gas concentration in the liquid will increase with time. If gas diffusion is slow compared to the initial bubble expansion rate there is an initial drop in the gas pressure inside the bubble as it expands. However, as the excess gas produced by the reaction diffuses into the bubble we see an increase in gas pressure (see Fig. 11). The bubble gas pressure only begins to fall once the reaction rate decreases and the gas concentration in the fluid decays. Increasing the diffusivity increases the rate at which gas is transported into the bubble. This produces an increase in the bubble gas pressure at early times and a consequent increase in the rate of bubble growth (Figs. 11 and 12).

Comparing Figs. 5 and 13 we see the effect of the polymerisation on the elastic stress. For a non-reacting system, Fig. 5, reducing the diffusivity (and hence the bubble growth rate) produced a much lower first

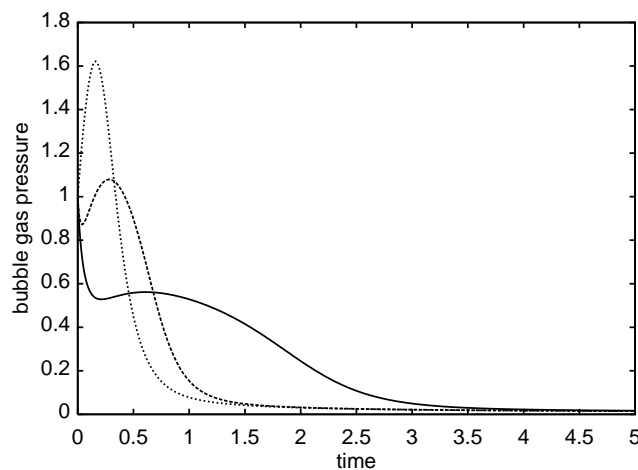


Fig. 11. Effect of diffusivity on dimensionless bubble gas pressure when $M = 10$. Solid line: $N = 9$; dashed line: $N = 90$; dotted line shows the limit of infinite diffusion.

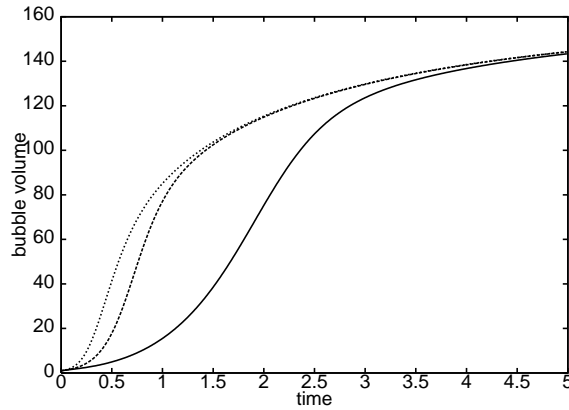


Fig. 12. Effect of diffusivity on bubble growth when $M = 10$. Solid line: $N = 9$; dashed line: $N = 90$; dotted line shows the limit of infinite diffusion.

normal stress difference. However, in Fig. 13, we see that the main effect of diffusivity is to delay the point of maximum first normal stress difference with relatively little change in the magnitude. Although a lower diffusivity reduces the bubble expansion rate at early times, it delays the maximum rate of expansion to times when the molecular weight is larger and so the fluid is more viscoelastic. Fig. 14 shows the evolution of the extent of reaction and the longest relaxation time, we see that the longest relaxation time diverges at the gel point.

In the three cases shown in Figs. 11–13, the final bubble volume is independent of diffusivity. In these cases, the rate of the reaction is sufficiently slow for the gas pressure to reach equilibrium before the gel point is reached. At faster reaction rates the gas bubble will not have reached its equilibrium size before gelation and so the equilibrium bubble volume will depend on the values of N and M (see Fig. 15). The asymptotes given by the limit of infinite diffusivity in Fig. 16 show that the ratio of the bubble expansion

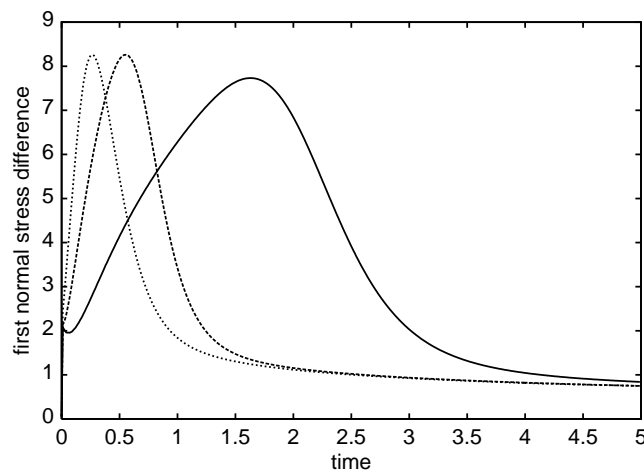


Fig. 13. Effect of diffusivity on the magnitude of the first normal stress difference, $|\gamma \sum G(k)(A_{rr}(k) - A_{\theta\theta}(k))|$, when $M = 10$. Solid line: $N = 9$; dashed line: $N = 90$; dotted line shows the limit of infinite diffusion.

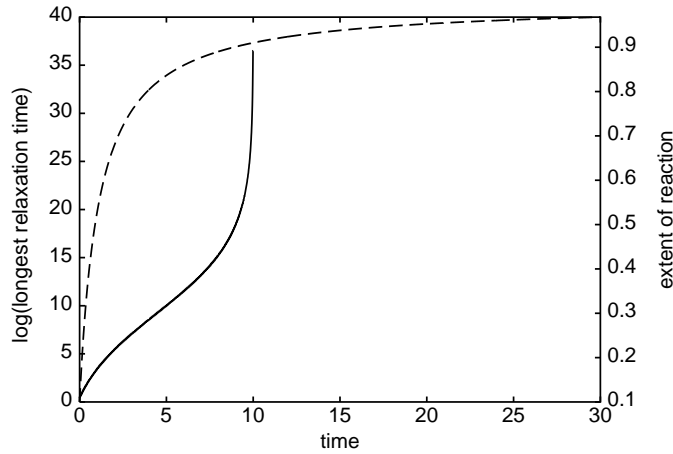


Fig. 14. The evolution of the longest relaxation time (solid line) and the extent of reaction (broken line).

rate to reaction rate, M dictates a maximum equilibrium volume. The ratio of the rate of gas diffusion to reaction rate, N , dictates the proportion of that volume achieved.

As the liquid gels the stretch in the modes with relaxation rates less than ϵ_{ch} does not relax back to the equilibrium state and so, in the absence of surface tension,

$$P_g \rightarrow -\frac{2}{3}\gamma \frac{d_r}{2} \left(\frac{\epsilon_{ch}}{\epsilon_x} \right)^{(1/2)d_r(v-1)} \int_0^X \frac{A_{rr} - A_{\theta\theta}}{x + u} dx.$$

Thus, the equilibrium bubble volume depends on the trapped gas pressure, $P_{g\infty}$, and

$$u_\infty = \frac{1 + \zeta\alpha_0 + \zeta\Phi(\alpha_\infty - \alpha_0 P_{g\infty})X}{1 + \zeta\alpha_0 P_{g\infty}}.$$

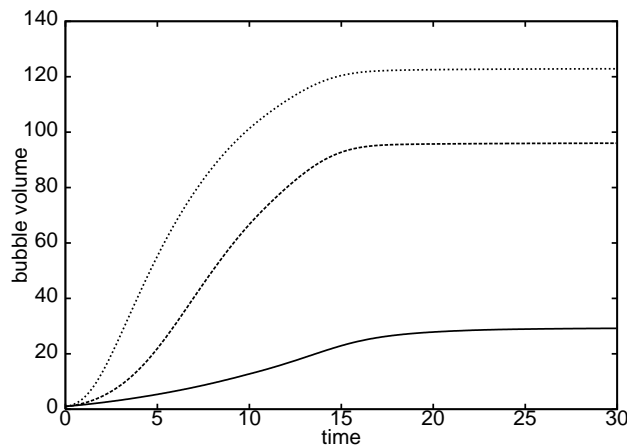


Fig. 15. Effect of diffusivity on bubble growth when $M = 1$ and $\gamma = 73.8$. Solid line: $N = 0.9$; dashed line: $N = 9$; dotted line shows the limit of infinite diffusion.

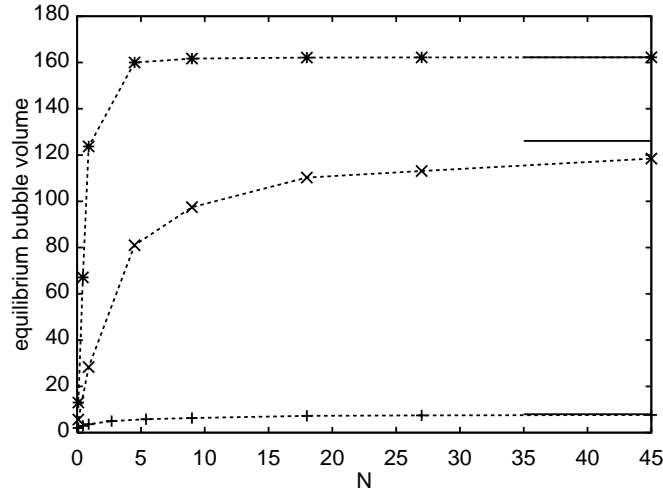


Fig. 16. Equilibrium bubble volume as a function of gas diffusivity, N , for different values of the ratio of bubble growth rate to reaction rate M : $M = 0.1$ (+); $M = 1$ (x); $M = 5$ (*). Solid lines indicate asymptotes for limit $N \rightarrow \infty$.

The bracketed term represents the gas which has diffused into the bubble: $\zeta H p_a \alpha_\infty$ is the number of moles per unit volume of gas generated during the reaction and $\zeta H p_a \alpha_0 p_{g\infty}$ is the number of moles per unit volume of gas remaining in the fluid at the end of the reaction.

Increasing γ increases the viscosity of the liquid throughout the reaction and so decreases the equilibrium bubble volume while increasing the magnitude of the first normal stress difference and the equilibrium gas pressure. This effect is much more pronounced at high reaction rates. Increasing α_0 , the extent of reaction when the bubble nucleates, increases the initial gas pressure in the bubble and so the equilibrium bubble volume at completion of the reaction is increased.

3.5. Justification of the full reacting model

In this section, we justify the complexity of our reacting model by comparing the results for bubble expansion with results generated by using two vastly simplified models.

The simplest model for a reacting fluid might be that of a generalised Newtonian fluid with viscosity that increases with the extent of reaction. We use a viscosity equivalent to the total viscosity of the full reacting model outlined above. As the reaction approaches the critical extent of reaction the longest relaxation time and viscosity diverge to infinity. The elasticity of the material allows the bubble to continue expanding beyond this point. If the fluid is modelled as Newtonian with increasing viscosity, the diverging viscosity would halt bubble expansion at the gel point. At low reaction rates most of the bubble expansion takes place before the gel point while the molecules are small and stress relaxes quickly. In these circumstances, the Newtonian model gives a reasonable approximation, particularly at early times. At high reaction rates, the molecules increase in size quickly and so the elasticity of the material becomes significant.

In order to improve the prediction without making the model very much more complex we devised a model that incorporates the early time accuracy of the generalised Newtonian model with the late time necessity for an elastic model. At early times, we use an increasing Newtonian viscosity, as above, with

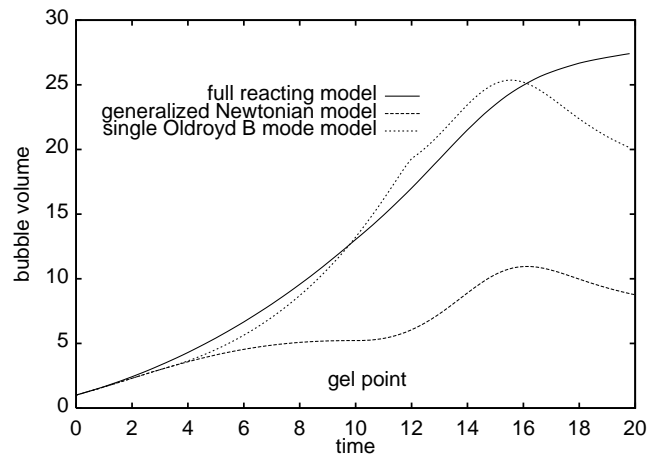


Fig. 17. Bubble expansion at high reaction rate to compare simplified models for a reacting fluid with the full reacting model. The ratio of initial expansion rate to reaction rate, $M = 1$.

no elastic contribution. At later times, the Newtonian viscosity remains constant and we introduce a single Oldroyd-B mode with increasing relaxation time equal to τ_{ch} and elastic modulus, G , fixed to give the correct viscosity. After the gel point, the gel mode is added by a second Oldroyd-B mode with infinite relaxation time. As the longest relaxation time drops, we revert to a decreasing Newtonian viscosity and no elastic contribution. At low reaction rates the point at which the elastic mode contributes can be adjusted to give a very close fit. However, at high reaction rates Fig. 17 shows that the predictions are still poor. The generalised Newtonian model gives a very poor fit due to the rapid increase in viscosity. Expansion starts up again after the gel point as the viscosity of the sol fraction decreases as an increasing fraction of the material becomes gel. The single Oldroyd-B mode model gives a slightly better fit until well after the gel point.

These models justify use of the full reacting model at high reaction rates while providing a fast approximate prediction of bubble expansion at low reaction rates.

4. Conclusion

In this paper, we have set out a practical model for the growth of bubbles in viscoelastic fluids driven by gas diffusion from the surrounding liquid. We link constitutive laws for the fluid rheology to a flow simulation for an expanding bubble.

For a non-reacting polymer in which the liquid rheology remains constant there are three important timescales that characterise bubble growth: the polymer relaxation time, a characteristic time for bubble growth in a viscous liquid, and the gas diffusion time. For viscoelastic effects to be important, the polymer relaxation time must be larger than the expansion timescale. Provided that this condition is satisfied, bubble growth can be divided into two classes: diffusion limited growth, where the growth rate is controlled by the diffusive transport of gas from the liquid; and stress limited growth, where the expansion rate is determined by the polymer relaxation rate.

In a reacting polymer system, there is a fourth timescale, the reaction time. This sets both the rate of gas production and the onset of gelation where the polymer relaxation time diverges. Most of the gas is produced in the early phase of the reaction, whereas the changes to the rheology are most significant when the reaction is near completion. If the reaction rate is fast relative to the timescale for bubble growth (set either by diffusion or fluid rheology) then gelation will freeze the structure before the stresses have relaxed or pressure decayed. If the reaction is relatively slow then the bubble will reach its equilibrium size before gelation takes place. Mora et al. [9] describe a foaming reaction in which 60% conversion is reached in about 2.5 min. This gives $c_\alpha = 0.01 \text{ s}^{-1}$ and, for the other parameters given in Table 4, bubble growth is controlled by the reaction.

At low reaction rates, a simple generalised Newtonian liquid model or a combination of a generalised Newtonian and Oldroyd-B model with increasing relaxation time give reasonable predictions for bubble growth in a gelling liquid. However, at high reaction rates the material properties change so rapidly that the large elastic stresses caused by the bubble expansion make a fluid model such as the one presented necessary.

In order to maintain simplicity in a highly complex system we have chosen to ignore many additional complications that arise in reaction injection moulding. We assumed a single species of reactant, whereas in many cases there are at least two. Our analysis assumes isothermal conditions, whereas in practice the synthesis reaction is often highly exothermic. Also, in addition to chemical gelation due to branching there may be phase separation that is thought to produce a physical gel [8,9]. This occurs before chemical gelation and so gives a gel point earlier in the reaction. Both these effects could be incorporated into the model and would be expected to modify the quantitative result. However, our model is able to capture the qualitative dependence of this highly complex system on the various parameters.

Acknowledgements

Sally Everitt would like to acknowledge the EPSRC and Huntsman Polyurethanes (an international business of Huntsman International LLC) for their financial support. We would also like to thank Don Jones for many useful discussions.

References

- [1] M. Amon, C. Denson, A study of the dynamics of foam growth: analysis of the growth of closely spaced spherical bubbles, *Polym. Eng. Sci.* 24 (13) (1984) 1026–1034.
- [2] A. Arafmanesh, S.G. Advani, Diffusion induced growth of a gas bubble in a viscoelastic fluid, *Rheol. Acta* 30 (1991) 274–283.
- [3] A. Arafmanesh, S.G. Advani, Non-isothermal bubble growth in polymeric foams, *Polym. Eng. Sci.* 35 (5) (1995) 252–260.
- [4] M.E. De Rosa, M. Mours, H.H. Winter, The gel point as reference state: a simple kinetic model for crosslinking polybutadiene via hydrosilation, *Polym. Gels Netw.* 5 (1997) 69–94.
- [5] M. Doi, S.F. Edwards, *Theory of Polymer Dynamics*, Oxford Science Publications/Clarendon Press, Oxford, 1986.
- [6] J.C. Gimel, T. Nicolai, D. Durand, J.M. Teuler, Structure and size distribution of percolating clusters. Comparison with gelling systems, *Eur. Phys. J. B* 12 (1999) 91–97.
- [7] C.J. Han, H.J. Yoo, Studies on structural foam filling. IV. Bubble growth during mould filling, *Polym. Eng. Sci.* 21 (9) (1981) 518–533.
- [8] C.W. Macosko, *Fundamentals of Reaction Injection Molding*, Hanser Publishers, 1989.

- [9] E. Mora, L.D. Artavia, C.W. Macosko, Modulus development during reactive polyurethane foaming, *J. Rheol.* 35 (5) (1991) 921–940.
- [10] M. Mours, H.H. Winter, Relaxation patterns of nearly critical gels, *Macromolecules* 29 (1996) 7221–7229.
- [11] F. Prochazka, T. Nicolai, D. Durand, Molar mass distribution of linear and branched polyurethane studied by size exclusion chromatography, *Macromolecules* 33 (2000) 1703–1709.
- [12] N.S. Ramesh, D.H. Rasmussen, G.A. Campbell, Numerical and experimental studies of bubble growth during the microcellular foaming process, *Polymer Eng. Sci.* 31 (1991) 1657–1664.
- [13] H. Randrianantoandro, T. Nicolai, D. Durand, F. Prochazka, Slow dynamics in gels, *J. Non-Newtonian Fluid Mech.* 67 (1996) 311–323.
- [14] M. Rubinstein, R.H. Colby, J.R. Gillmor, Dynamic scaling for polymer gelation, in: F. Tanaka, M. Doi, T. Ohta (Eds.), *Space–Time Organisation in Macromolecular Fluids*, Springer, Berlin, 1989, pp. 66–74.
- [15] M.A. Shafi, R.W. Flumerfelt, Initial bubble growth in polymer foam processes, *Chem. Eng. Sci.* 52 (4) (1997) 627–633.
- [16] M.A. Shafi, K. Joshi, R.W. Flumerfelt, Bubble size distribution in freely expanded polymer foams, *Chem. Eng. Sci.* 52 (4) (1997) 635–644.
- [17] D. Stauffer, A. Ahaony, *Introduction to Percolation Theory*, revised second ed., Taylor & Francis, London, 1994.
- [18] J.R. Street, The rheology of phase growth in elastic liquids, *Trans. Soc. Rheol.* 12 (1) (1968) 103–131.
- [19] I. Tanasawa, W. Yang, Dynamic behavior of a gas bubble in viscoelastic fluids, *J. Appl. Phys.* 41 (11) (1970) 4526–4531.
- [20] R. Ting, Viscoelastic effect of polymers on single bubble dynamics, *AIChE J.* 21 (4) (1975) 810–813.
- [21] H.H. Winter, M. Mours, Rheology of polymers near liquid–solid transitions, *Adv. Polym. Sci.* 134 (1997) 165–234.